

# Observation-Time-Induced Crossover from Fluctuating Diffusivity

Masahiro Shirataki<sup>1</sup> and Takuma Akimoto<sup>1,\*</sup>

<sup>1</sup>*Department of Physics and Astronomy, Tokyo University of Science, Noda, Chiba 278-8510, Japan*

(Dated: December 8, 2025)

A dynamical transition—seen as a sudden increase in the mean-squared displacement at a characteristic temperature that depends on the observation time—is widely reported in neutron-scattering experiments and molecular dynamics simulations of hydrated proteins. However, its physical origin remains elusive. We show that fluctuating diffusivity in a Langevin framework leads to an observation-time-induced crossover, where the effective diffusion coefficient exhibits a temperature-dependent transition whose crossover point shifts with observation time. Analytical and numerical analyses reveal the mechanism of this crossover and delineate the conditions under which it emerges. Our findings provide a unified nonequilibrium interpretation for observation-time-induced crossover, and suggest that the protein dynamical transition can be viewed as an instance of this general crossover mechanism.

Hydrated proteins exhibit a sharp increase in the mean-squared displacement (MSD) around 200-240 K, a well-known feature termed the protein dynamical transition (DT) [1–11]. Strikingly, neutron-scattering experiments show that the apparent transition temperature depends on the instrumental resolution [4, 8, 10, 11], indicating that the DT is not a true thermodynamic transition but an observation-time-dependent crossover. Relaxation processes of the hydration-water hydrogen-bond network are believed to set the relevant timescales [12], but a general physical mechanism explaining the observed dependence on the observation window has remained elusive.

Fluctuating diffusivity arises naturally in protein diffusion, where complex conformational dynamics—including long-term memory and folding-unfolding transitions—continuously modulate the hydrodynamic radius [13–17]. A Stokes-Einstein-like relation [18] implies that these structural fluctuations directly generate temporal variations of the instantaneous diffusivity. Analogous mechanisms appear in polymer systems: in the reptation model, for example, center-of-mass diffusion is controlled by fluctuations of the end-to-end vector [19–21], and fluctuating mobility also arises in other coarse-grained polymer models [22].

Such temporal variations of mobility lead to the striking phenomenon of Brownian yet non-Gaussian diffusion (BYNGD), in which the MSD grows linearly in time but the displacement distribution remains non-Gaussian. BYNGD has been reported in complex environments such as cytoplasm, polymer networks, and glassy systems [23–30]. The diffusing-diffusivity framework has been extensively investigated in this context, including studies of non-Gaussian displacement distributions, first-passage-time statistics, and ergodicity breaking [21, 22, 31–40], establishing fluctuating diffusivity as a central mechanism of anomalous transport.

While most previous studies focused on displacement statistics, we address a different facet of fluctuating diffusivity: the temperature dependence of the effective

diffusion coefficient under finite observation time. We show that, under nonequilibrium initial conditions, a sharp crossover in the temperature-dependent effective diffusivity naturally emerges, with the crossover point shifting systematically on the observation time. This observation-time-induced crossover is distinct from BYNGD and from equilibrium phase transitions. We demonstrate that it arises generically from the interplay of fluctuating diffusivity, temperature-dependent relaxation, and finite-time observation.

To clarify this mechanism, we study a double-well-controlled diffusing diffusivity (DWCDD) model, where the instantaneous diffusivity evolves stochastically in a double-well potential, mimicking conformational transitions between folded and unfolded states. For analytical tractability, we reduce this model to a coarse-grained two-state representation that captures the essential features of the effective diffusivity. Through analytical and numerical approaches, we establish the necessary conditions for the observation-time-induced crossover and provide a minimal framework for interpreting dynamical transitions in complex systems. Our results highlight the importance of observation-time effects in the analysis of transport phenomena in biomolecular and soft-matter experiments.

*Model.*—In the Langevin equation with fluctuating diffusivity, the diffusion coefficient  $D(t)$  is a stochastic process that varies in time, reflecting temporal heterogeneity in the medium. The particle position  $x(t)$  then evolves according to the stochastic differential equation:

$$\frac{dx(t)}{dt} = \sqrt{2D(t)}\xi(t), \quad (1)$$

where  $\xi(t)$  is a Gaussian white noise satisfying

$$\langle \xi(t) \rangle = 0, \quad \langle \xi(t)\xi(t') \rangle = \delta(t - t'). \quad (2)$$

Although the diffusivity  $D(t)$  originates from environmental fluctuations or from internal degrees of freedom of the particle—such as conformational changes—we assume that  $D(t)$  and  $\xi(t)$  are statistically independent.

This assumption reflects a separation of timescales: the slow, structured environmental or conformational dynamics that modulate mobility are captured by  $D(t)$ , while  $\xi(t)$  represents fast, memoryless thermal noise. In this sense, the time evolution of the diffusivity is treated as an external stochastic modulation, independent of the instantaneous thermal driving force acting on the particle.

*Double-well-controlled diffusing diffusivity model.*—To capture the impact of time-dependent diffusivity—such as that arising from protein conformational fluctuations—we adopt the DWCD model, in which  $D(t)$  evolves continuously under a double-well potential. This framework naturally captures smooth transitions between low- and high-diffusivity states, reminiscent of folded-unfolded transitions that modulate the effective mobility of proteins. In the DWCD model, the particle's diffusion coefficient  $D(t)$  is assumed to follow a Stokes–Einstein-type relation [18, 41],

$$D(t) = \frac{k_B T}{r(t)}, \quad (3)$$

where  $T$  is the temperature,  $r(t)$  represents the instantaneous gyration radius of the particle, and  $k_B$  is the Boltzmann constant. The stochastic dynamics is governed by an overdamped Langevin equation in a double-well potential, modeling conformational fluctuations between compact and extended states [41, 42]:

$$\gamma \frac{dr(t)}{dt} = -\frac{\partial V(r)}{\partial r} + \sqrt{2\gamma k_B T} \eta(t), \quad (4)$$

where  $\gamma$  is the friction coefficient,  $V(r)$  is a double-well potential, and  $\eta(t)$  is Gaussian white noise satisfying

$$\langle \eta(t) \rangle = 0, \quad \langle \eta(t) \eta(t') \rangle = \delta(t - t'). \quad (5)$$

The noise  $\eta(t)$  is assumed to be statistically independent of  $\xi(t)$ ,  $x(t)$  and  $r(t)$ . In this model, we employ a double-well potential of the form  $V(r) = ar^4 + br^3 + cr^2 + dr + e$ . The parameters are set to  $a = 0.05$ ,  $b = -0.6$ ,  $c = 2.3$ ,  $d = -3$ , and  $e = 1.25$ . This potential exhibits two minima located at  $r_+ = 1$  and  $r_- = 5$ , and is symmetric about the potential barrier at  $r_M = 3$ . To avoid unphysical values such as negative or extremely large diffusion coefficients, a reflecting boundary is imposed at boundaries at  $r = 0.1$  and  $r = 7$ . The lower boundary is physically motivated by interpreting  $r(t)$  as the gyration radius of the molecule: when the system reaches a highly compact conformation ( $r \sim 0.1$ ), strong steric repulsion is assumed to arise, preventing further compression and effectively pushing  $r(t)$  to expand. The upper boundary at  $r = 7$  is introduced to prevent unbounded expansion at high temperatures, ensuring physical plausibility of the conformational fluctuations. Figure 1 shows the time evolution of the diffusion coefficient  $D(t)$  and the corresponding particle trajectory  $x(t)$  in the DWCD model.

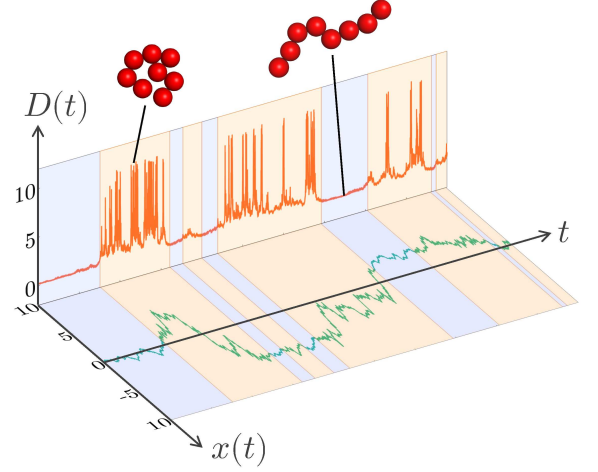


FIG. 1. Particle trajectory  $x(t)$  and corresponding time-dependent diffusion coefficient  $D(t)$  in the DWCD model.

To explore the DT, we consider non-equilibrium initial conditions in which the system starts in the low-diffusivity state. Specifically in the DWCD model, the initial value of the conformational variable is set to  $r(0) = r_-$ , where  $r_-$  corresponds to the right minimum of the double-well potential and thus represents the low-diffusivity state. In this way, we can investigate the nonequilibrium character of the MSD and how it reflects the transient dynamical behavior arising from the initial condition.

*Mapping onto two-state model.*—To elucidate its essential features, we describe its dynamics using a coarse-grained two-state representation. In this description, the diffusivity alternates between two states, denoted as the  $+$  and  $-$  states, characterized by radii  $r_+$  and  $r_-$  with  $r_- > r_+$ . The corresponding diffusion coefficients are given by

$$D_{\pm} = \frac{k_B T}{r_{\pm}}, \quad (6)$$

which serves as the discrete analogue of Eq. (3).

This two-state picture becomes accurate when the temperature is low compared to the barrier height of the double-well potential ( $\Delta U/k_B T \gg 1$ ), so that escape events between the wells are rare and can be treated as statistically independent. In this Arrhenius regime, the continuous dynamics of the DWCD model can therefore be coarse-grained into two discrete diffusivity states. Each state persists for a random sojourn time  $\tau$ , drawn from a state-specific probability density function (PDF)  $\rho_{\pm}(\tau)$ . For analytical tractability, we assume exponential sojourn-time distributions, corresponding to a Markovian switching process. Specifically, we set

$$\rho_{\pm}(\tau) = \frac{1}{\mu_{\pm}} e^{-\tau/\mu_{\pm}}, \quad \tau \geq 0, \quad (7)$$

where  $\mu_+$  and  $\mu_-$  denote the mean sojourn times in the  $+$  and  $-$  states, respectively.

In the DWCD model, the variable  $r(t)$  fluctuates within a double-well potential. Since the initial condition is set at the right minimum,  $r = r_-$ , the system initially remains in the low-diffusivity basin. As temperature increases, the particle occasionally acquires enough thermal energy to escape from this well and begins to explore both minima at  $r_-$  and  $r_+$ . The distribution of  $r(t)$  then gradually relaxes toward the equilibrium distribution. In this regime, the sojourn times in the two wells can be interpreted as temperature-dependent escape times from the corresponding minima. Thus, the dynamics effectively reduce to stochastic switching between the two discrete states  $r = r_+$  and  $r = r_-$ , which justifies mapping the DWCD model onto the coarse-grained two-state model.

From the Arrhenius law, the mean sojourn times in the  $+$  and  $-$  states are given by

$$\mu_{\pm} \sim 2\alpha_{\pm}\delta\pi \exp\left(\frac{V(r_M) - V(r_{\pm})}{k_B T}\right), \quad (8)$$

valid in the activated regime  $\Delta U/(k_B T) \gg 1$ , where  $\Delta U = V(r_M) - V(r_{\pm})$  is the barrier height. Here,  $r_+$  and  $r_-$  denote the positions of the left and right minima, respectively, and  $r_M$  is the position of the barrier top. The prefactors  $\alpha_{\pm}$  are determined by the curvatures of the potential near  $r = r_{\pm}$ .

*Observation-time-induced crossover.*—In the two-state model, the MSD of a particle, starting from  $x(0) = 0$ , can be computed as [40, 43]:

$$\langle x^2(t) \rangle = 2 \int_0^t \langle D(t') \rangle dt'. \quad (9)$$

In equilibrium, the ensemble average of  $D(t)$  becomes time-independent and equals

$$D_{\text{eq}} = \frac{\mu_+ D_+ + \mu_- D_-}{\mu_+ + \mu_-}, \quad (10)$$

the stationary mean determined by the equilibrium probabilities of the two states. In contrast, under nonequilibrium initial conditions, the ensemble average  $\langle D(t) \rangle$  acquires explicit time dependence. It can be expressed as

$$\langle D(t) \rangle = D_- + (D_+ - D_-)p_+(t), \quad (11)$$

where  $p_+(t)$  is the probability that the system is in the fast state ( $+$ ) at time  $t$ . Since the system is initialized in the slow state,  $p_+(0) = 0$ , and the time evolution of  $p_+(t)$  follows from standard renewal-theory results [40, 44–46].

Starting from the slow state, the time-dependent average diffusivity is given by

$$\langle D(t) \rangle = D_{\text{eq}} - (D_+ - D_-) \frac{\tilde{\mu}}{\mu_-} e^{-t/\tilde{\mu}}, \quad (12)$$

where  $\tilde{\mu} \equiv \mu_+ \mu_- / (\mu_+ + \mu_-)$  is the effective relaxation time of the two-state dynamics. Using Eq. (9) and defining effective diffusion coefficient as

$$D_{\text{eff}}(t) \equiv \frac{\langle x^2(t) \rangle}{2t}, \quad (13)$$

we obtain

$$D_{\text{eff}}(t) = D_{\text{eq}} - (D_+ - D_-) \frac{\tilde{\mu}^2}{\mu_- t} \left(1 - e^{-t/\tilde{\mu}}\right). \quad (14)$$

Equation (14) describes how the effective diffusivity evolves from its initial nonequilibrium value toward the equilibrium diffusivity  $D_{\text{eq}}$ . The first term gives the long-time limit, while the second term quantifies the transient decay originating from the initial slow state. The crossover is governed by the characteristic relaxation time  $\tilde{\mu}(T)$ : the effective diffusivity transitions smoothly from its initial to its equilibrium value when the observation time becomes comparable to  $\tilde{\mu}(T)$ .

For a symmetric double-well potential centered at  $r = r_M$ , substituting the mean escape times  $\mu_{\pm}$  from Eq. (8) into Eq. (14) yields the effective diffusion coefficient of the DWCD model as

$$D_{\text{eff}}(t) = D_- + \frac{D_+ - D_-}{2} \left[1 - \frac{1 - \exp(-t/\kappa(T))}{t/\kappa(T)}\right], \quad (15)$$

where  $\kappa(T) \equiv \alpha \delta \pi e^{\frac{\Delta U}{k_B T}}$  is the characteristic relaxation time. Here,  $\Delta U = V(r_M) - V(r_{\pm})$  denotes the barrier height, and symmetry implies  $\alpha \equiv \alpha_+ = \alpha_-$ . Equation (15) reveals how the effective diffusivity evolves over time as the system relaxes between the two diffusivity states separated by an energy barrier  $\Delta U$ . The temperature dependence of  $\kappa(T)$  follows an Arrhenius form, increasing exponentially with  $\Delta U$  and decreasing with temperature. For short observation times  $t \ll \kappa(T)$ , the expansion  $1 - e^{-t/\kappa(T)} \simeq t/\kappa(T)$  gives  $D_{\text{eff}}(t) \simeq D_-$ , indicating that the system remains in its initial low-diffusivity state. For long times  $t \gg \kappa(T)$ , the exponential term vanishes and  $D_{\text{eff}}(t)$  approaches the equilibrium value  $(D_+ + D_-)/2$ . Thus, Eq. (15) captures the observation-time-dependent crossover from nonequilibrium to equilibrium diffusivity, governed by thermally activated transitions between conformational states.

Figure 2 shows the temperature dependence of the effective diffusion coefficient  $D_{\text{eff}}$  in the DWCD model. A clear transition in  $D_{\text{eff}}$  is observed with increasing temperature, and the transition temperature systematically depends on the observation time. Theoretical predictions from Eq. (15) (solid lines) are in excellent agreement with the simulation results (symbols), confirming that the observation-time-induced crossover arises from thermally activated transitions between the two diffusivity states.

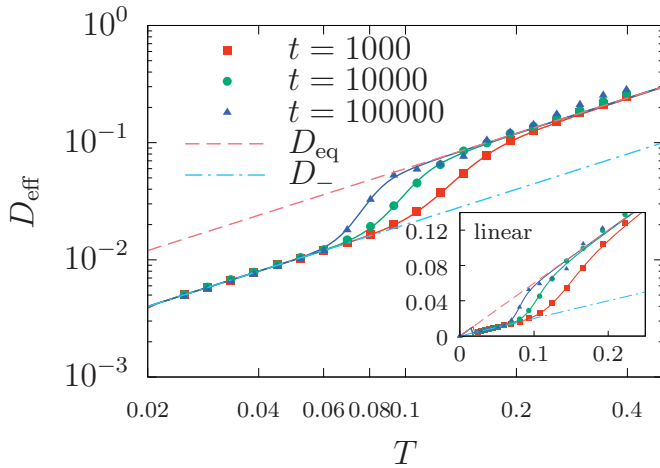


FIG. 2. Temperature-dependent effective diffusion coefficient for different observation times in the DWCD model. Symbols indicate simulation results, dashed lines represent the initial and equilibrium diffusion coefficients, and solid lines show the theoretical prediction given by Eq. (15). Inset: linear-scale zoom around  $T < 0.2$ .

*Conditions for the emergence of observation-time-induced crossover.*—We now discuss the conditions under which a dynamical transition emerges, based on the results presented above. Our analysis indicates that the observation-time-induced crossover is governed by the following three conditions:

- (i) The instantaneous diffusivity fluctuates in time.
- (ii) The relaxation time of the diffusivity depends on temperature.
- (iii) The system is initially out of equilibrium.

The second condition is essential, as the apparent transition temperature depends on the observation time; equivalently, the diffusivity must switch between states on a temperature-dependent timescale. Because condition (i) is a prerequisite for the others, our discussion focuses on (ii) and (iii). Using representative numerical examples, we confirm in the Supplemental Material (SM) that these three conditions are jointly necessary for the emergence of the crossover.

*Extraction of relaxation dynamics from trajectory data.*—To illustrate how the present framework enables the extraction of information about underlying conformational dynamics, we discuss how relaxation properties can be inferred from finite-time measurements of effective diffusivity. Observation-time-induced crossovers arise only when the system is initialized in a nonequilibrium state; in the diffusivity model, this is implemented by fixing the initial radius in one of the basins, such as the low-diffusivity minimum. Molecular-dynamics (MD) simulations of proteins, however, typically begin from an equilibrium ensemble [18]. When relaxation dynamics are to

be probed, the initial state can nevertheless be controlled explicitly—for example, by selecting configurations from a particular basin (compact or expanded) or by briefly equilibrating the system at a chosen temperature. Thus, although observing the crossover requires specifying an initial basin, such initialization can be straightforwardly imposed in MD simulations.

The effective diffusivity contains direct information about the underlying conformational landscape. For a double-well-type landscape, the ratio of radii in the two basins is related to the diffusivity ratio through

$$\frac{r_-}{r_+} = 2 \frac{D_{\text{eq}}}{D_-} - 1, \quad (16)$$

which is exact for a symmetric potential and remains a good approximation whenever the escape times from the two minima are of the same order. Thus, the magnitude of conformational change can be inferred from the measured diffusivity contrast. MD simulations typically report radius-of-gyration changes of about  $r_-/r_+ \simeq 1.2$  [18]; inserting this value gives  $D_{\text{eq}}/D_- \simeq 1.1$ . Hence even a modest ( $\sim 10\%$ ) change in effective diffusivity signals a realistic conformational transition.

The temperature dependence of the crossover also encodes the energy barrier. A transition becomes apparent when the observation time  $t_{\text{obs}}$  matches the relaxation time  $\kappa(T)$  governing interconversion between basins. For thermally activated dynamics,

$$t_{\text{obs}} \sim \kappa(T_c) = \alpha \delta \pi \exp\left(\frac{\Delta U}{k_B T_c}\right), \quad (17)$$

so that

$$\log(t_{\text{obs}}) \sim \frac{\Delta U}{k_B} \frac{1}{T_c} + \log(\alpha \delta \pi). \quad (18)$$

Thus, by measuring the shift of the apparent crossover temperature with observation time, one can directly estimate the conformational barrier  $\Delta U$ .

Together, these relations show that finite-time diffusivity data provide quantitative access to the characteristic radii and barrier heights governing conformational relaxation—even when only trajectory-level observables are available.

*Relation to the dynamical transition.*—The protein DT observed in neutron-scattering experiments emerges when the relaxation times of internal motions dominated by hydration-water become comparable to the instrumental observation window. Our results show that the same timescale-matching condition underlies the observation-time-induced crossover produced by fluctuating diffusivity.

A key requirement for this crossover is that the system is initially biased away from the equilibrium diffusivity distribution. In DT experiments, samples are not prepared in a deliberately chosen nonequilibrium basin as



in our protocol. Nevertheless, the relevant internal degrees of freedom often relax on timescales much longer than the picosecond-nanosecond window probed by neutron scattering. Thus, after a temperature change these modes cannot fully equilibrate within the measurement time and remain biased toward their pre-transition state, providing an effective nonequilibrium initial condition. Importantly, this situation persists even when a finite equilibration time  $t_{\text{eq}}$  is allowed before measurement: as long as  $t_{\text{eq}}$  and the observation window are not sufficient to erase the initial bias, finite-time measurements probe a partially relaxed state and the crossover remains observable (see SM for numerical confirmation). Therefore, DT measurements generically realize an effective nonequilibrium initial condition for the relevant internal modes, so the requirement for the observation-time-induced crossover is naturally met.

This picture also implies a heating-cooling asymmetry. Upon heating from a low-mobility basin, relaxation is slow at low temperatures, so a nonequilibrium bias persists during the measurement and the observation-time-induced crossover appears. By contrast, at high temperature the diffusivity relaxes rapidly and its distribution quickly reaches the stationary form. Once equilibrated, subsequent cooling does not regenerate a meaningful nonequilibrium bias; rather, the system tracks the equilibrium distribution quasi-adiabatically at each temperature. Therefore the nonequilibrium initial condition required for the crossover is absent in the cooling protocol, and no crossover is expected (see SM for numerical confirmation). This scenario suggests an experimental asymmetry: DT should be suppressed, or even absent, under cooling protocols in which the system remains near equilibrium at each temperature.

**Conclusion.**—In summary, we have shown that fluctuating diffusivity in the Langevin framework generically leads to an observation-time-induced crossover, in which the effective diffusion coefficient exhibits a sharp, temperature-dependent transition whose crossover point shifts systematically with the observation time. By combining analytical treatments of a coarse-grained two-state model with numerical simulations of a DWCD model, we identified the minimal conditions required for the emergence of such transitions: (i) temporal fluctuations of diffusivity, (ii) temperature-dependent relaxation times, and (iii) nonequilibrium initial conditions.

**Acknowledgements.**—The authors thank Tomoshige Miyaguchi and Eiji Yamamoto for fruitful discussions. T.A. was supported by JSPS Grant-in-Aid for Scientific Research (No. C 21K033920).

---

\* takuma@rs.tus.ac.jp

[1] W. Doster, S. Cusack, and W. Petry, *Nature* **337**, 754

- (1989).
- [2] W. Doster, S. Cusack, and W. Petry, *Phys. Rev. Lett.* **65**, 1080 (1990).
  - [3] A. L. Tournier and J. C. Smith, *Phys. Rev. Lett.* **91**, 208106 (2003).
  - [4] T. Becker, J. A. Hayward, J. L. Finney, R. M. Daniel, and J. C. Smith, *Biophysical Journal* **87**, 1436 (2004).
  - [5] J. Roh, J. Curtis, S. Azzam, V. Novikov, I. Peral, Z. Chowdhuri, R. Gregory, and A. P. Sokolov, *Biophys. J.* **91**, 2573 (2006).
  - [6] T. Becker and J. C. Smith, *Phys. Rev. E* **67**, 021904 (2003).
  - [7] D. Vural, L. Hong, J. C. Smith, and H. R. Glyde, *Phys. Rev. E* **88**, 052706 (2013).
  - [8] W. Doster, *Eur. Biophys. J.* **37**, 591 (2008).
  - [9] W. Doster, *Biochim. Biophys. Acta* **1804**, 3 (2010).
  - [10] S. Magazú, F. Migliardo, and A. Benedetto, *J. Phys. Chem. B* **115**, 7736 (2011).
  - [11] K. Ngai, S. Capaccioli, and A. Paciaroni, *Biochim. Biophys. Acta* **1861**, 3553 (2017).
  - [12] G. Schiro, Y. Fichou, F.-X. Gallat, K. Wood, F. Gabel, M. Moulin, M. Härtlein, M. Heyden, J.-P. Colletier, A. Orecchini, *et al.*, *Nat. Commun.* **6**, 6490 (2015).
  - [13] H. Yang, G. Luo, P. Karnchanaphanurach, T.-M. Louie, I. Rech, S. Cova, L. Xun, and X. S. Xie, *Science* **302**, 262 (2003).
  - [14] S. C. Kou and X. S. Xie, *Phys. Rev. Lett.* **93**, 180603 (2004).
  - [15] W. Min, G. Luo, B. J. Cherayil, S. C. Kou, and X. S. Xie, *Phys. Rev. Lett.* **94**, 198302 (2005).
  - [16] E. Yamamoto, T. Akimoto, Y. Hirano, M. Yasui, and K. Yasuoka, *Phys. Rev. E* **89**, 022718 (2014).
  - [17] X. Hu, L. Hong, M. Dean Smith, T. Neusius, X. Cheng, and J. C. Smith, *Nat. Phys.* **12**, 171 (2016).
  - [18] E. Yamamoto, T. Akimoto, A. Mitsutake, and R. Metzler, *Phys. Rev. Lett.* **126**, 128101 (2021).
  - [19] M. Doi and S. Edwards, *J. Chem. Soc., Faraday Trans. 2* **74**, 1789 (1978).
  - [20] M. Doi and S. F. Edwards, *The Theory of Polymer Dynamics* (Oxford University Press, Oxford, 1986).
  - [21] T. Uneyama, T. Miyaguchi, and T. Akimoto, *Phys. Rev. E* **92**, 032140 (2015).
  - [22] T. Miyaguchi, *Phys. Rev. E* **96**, 042501 (2017).
  - [23] B. Wang, S. M. Anthony, S. C. Bae, and S. Granick, *Proc. Natl. Acad. Sci. U.S.A.* **106**, 15160 (2009).
  - [24] B. Wang, J. Kuo, S. C. Bae, and S. Granick, *Nat. Mater.* **11**, 481 (2012).
  - [25] K. He, F. Babaye Khorasani, S. T. Retterer, D. K. Thomas, J. C. Conrad, and R. Krishnamoorti, *ACS Nano* **7**, 5122 (2013).
  - [26] S. Bhattacharya, D. K. Sharma, S. Saurabh, S. De, A. Sain, A. Nandi, and A. Chowdhury, *J. Phys. Chem. B* **117**, 7771 (2013).
  - [27] J. Guan, B. Wang, and S. Granick, *ACS Nano* **8**, 3331 (2014).
  - [28] G. Kwon, B. J. Sung, and A. Yethiraj, *J. Phys. Chem. B* **118**, 8128 (2014).
  - [29] J. M. Miotto, S. Pigolotti, A. V. Chechkin, and S. Roldán-Vargas, *Phys. Rev. X* **11**, 031002 (2021).
  - [30] F. Rusciano, R. Pastore, and F. Greco, *Phys. Rev. Lett.* **128**, 168001 (2022).
  - [31] T. Akimoto, J.-H. Jeon, R. Metzler, T. Miyaguchi, T. Uneyama, and E. Yamamoto, *arxiv:2509.12571* (2025).
  - [32] M. V. Chubynsky and G. W. Slater, *Phys. Rev. Lett.*

- 113**, 098302 (2014).
- [33] A. V. Chechkin, F. Seno, R. Metzler, and I. M. Sokolov, Phys. Rev. X **7**, 021002 (2017).
  - [34] V. Sposini, A. V. Chechkin, F. Seno, G. Pagnini, and R. Metzler, New J. Phys. **20**, 043044 (2018).
  - [35] T. Miyaguchi, T. Uneyama, and T. Akimoto, Phys. Rev. E **100**, 012116 (2019).
  - [36] V. Sposini, S. Nampoothiri, A. Chechkin, E. Orlandini, F. Seno, and F. Baldovin, Phys. Rev. Lett. **132**, 117101 (2024); Phys. Rev. E **109**, 034120 (2024).
  - [37] P. Massignan, C. Manzo, J. A. Torreno-Pina, M. F. García-Parajo, M. Lewenstein, and J. G. J. Lapeyre, Phys. Rev. Lett. **112**, 150603 (2014).
  - [38] T. Akimoto and E. Yamamoto, Phys. Rev. E **93**, 062109 (2016).
  - [39] T. Akimoto and E. Yamamoto, J. Stat. Mech. **2016**, 123201 (2016).
  - [40] T. Miyaguchi, T. Akimoto, and E. Yamamoto, Phys. Rev. E **94**, 012109 (2016).
  - [41] M. Kimura and T. Akimoto, Phys. Rev. E **106**, 064132 (2022).
  - [42] M. Shimizu, T. Miyaguchi, E. Yamamoto, and T. Akimoto, J. Chem. Phys. **163** (2025).
  - [43] T. Akimoto and E. Yamamoto, Phys. Rev. E **93**, 062109 (2016).
  - [44] D. R. Cox, *Renewal theory* (Methuen, London, 1962).
  - [45] C. Godrèche and J. M. Luck, J. Stat. Phys. **104**, 489 (2001).
  - [46] T. Akimoto, Phys. Rev. E **108**, 054113 (2023).

# Supplemental Material for *Observation-Time-Induced Crossover from Fluctuating Diffusivity*

Masahiro Shirataki<sup>1</sup> and Takuma Akimoto<sup>1,\*</sup>

<sup>1</sup>*Department of Physics and Astronomy, Tokyo University of Science, Noda, Chiba 278-8510, Japan*

(Dated: December 8, 2025)

## CONTENTS

I. Breakdown of Observation-Time-Induced Crossover	1
II. Observation-Time-Induced Crossover in Nonequilibrium Steady States (Three-State Model)	2
III. Asymmetric Double-Well Control of Diffusing Diffusivity	3
IV. Effect of The Equilibration Time	4
V. Heating-cooling Asymmetry in The Double-well Controlled Diffusing Diffusivity Model	5

## I. BREAKDOWN OF OBSERVATION-TIME-INDUCED CROSSOVER

Figure S1 demonstrates the necessity of conditions (i)-(iii) for the emergence of the observation-time-induced crossover, using two representative models. Panel (a) shows the result for the two-state model, where the mean sojourn times are set to be independent of temperature. In this case, although the instantaneous diffusivity fluctuates and switches between two discrete diffusion coefficients, the switching timescale remains temperature independent. As a result, condition (ii) is violated, and no observation-time-induced crossover appears. Panel (b) presents results for the diffusing diffusivity model, in which the potential is replaced by a harmonic approximation around  $r = r_-$ , eliminating bistability and thus suppressing diffusivity switching. In this model, transitions between distinct conformational states are absent, and condition (ii) is again not satisfied, and the observation-time-induced crossover does not emerge. Panel (c) examines the role of nonequilibrium initial conditions, corresponding to condition (iii). Here, the system is initialized with  $r$  sampled from the equilibrium distribution. In this case, there is no observation-time-induced crossover. Because the dynamical transition relies on relaxation from a nonequilibrium state, its emergence requires that the system be initially prepared out of equilibrium. Taken together, these results confirm that both

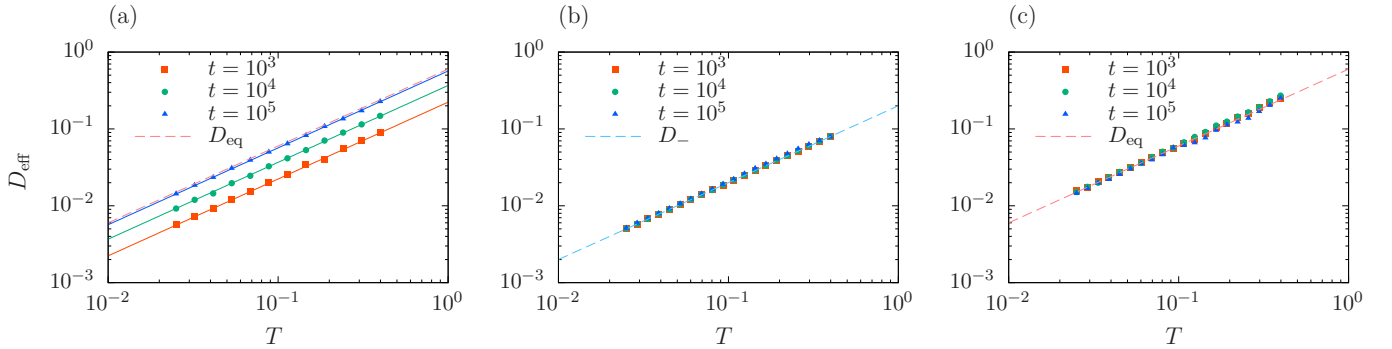


FIG. S1. Temperature-dependent effective diffusion coefficient for different observation times. (a) Two-state model, where the mean sojourn time  $\mu$  is temperature independent. (b) Diffusing-diffusivity model where the particle radius  $r$  evolves under a harmonic potential. (c) Double-well-controlled diffusing-diffusivity model with the initial condition of  $r$  sampled from the equilibrium distribution.

\* takuma@rs.tus.ac.jp

temperature-dependent relaxation and nonequilibrium initial conditions are indispensable for the emergence of the observation-time-induced crossover.

## II. OBSERVATION-TIME-INDUCED CROSSOVER IN NONEQUILIBRIUM STEADY STATES (THREE-STATE MODEL)

In this section, we extend the two-state model to a three-state model and show that a dynamical crossover arises even in cases where the instantaneous diffusion coefficient does not converge to its equilibrium value. The instantaneous diffusion coefficient takes three discrete values

$$D(t) \in \{D_1, D_2, D_3\}, \quad D_3 > D_2 > D_1. \quad (\text{A1})$$

Furthermore, the transition probabilities between states are specified by the transition matrix

$$P = \begin{pmatrix} 0 & \frac{1}{3} & \frac{2}{3} \\ \frac{2}{3} & 0 & \frac{1}{3} \\ \frac{1}{3} & \frac{2}{3} & 0 \end{pmatrix} \quad (\text{A2})$$

Here,  $P_{ij}$  denotes the probability of transitioning from state  $i$  to state  $j$ . The sojourn time in each state is modeled, as in the two-state model, by the exponential distribution

$$\rho(\tau) = \frac{1}{\mu} e^{-\tau/\mu}, \quad \tau \geq 0. \quad (\text{A3})$$

Here,  $\mu$  denotes the mean residence time in each states and is assumed to follow an Arrhenius-type temperature dependence given by

$$\mu(T) = \tau_0 \exp\left(\frac{\Delta U}{k_B T}\right). \quad (\text{A4})$$

Here,  $\tau_0$  is a characteristic residence time that is independent of  $\Delta U$  and  $T$ . As the initial condition, we set the instantaneous diffusion coefficient to  $D(0) = D_1$ .

Under the nonequilibrium initial condition, the instantaneous diffusion coefficient can be expressed as

$$\langle D(t) \rangle = D_1 + (D_2 - D_1) p_2(t) + (D_3 - D_1) p_3(t), \quad (\text{A5})$$

where  $p_2(t)$  and  $p_3(t)$  are the probabilities of finding the system in states 2 and 3 at time  $t$ , respectively. Using renewal theory, the probabilities are obtained as

$$p_2(t) = \frac{1}{3} - \frac{2}{3} \exp\left(-\frac{3}{2} \frac{t}{\mu}\right) \sin\left(\omega t + \frac{\pi}{6}\right), \quad (\text{A6})$$

$$p_3(t) = \frac{1}{3} + \frac{2}{3} \exp\left(-\frac{3}{2} \frac{t}{\mu}\right) \sin\left(\omega t - \frac{\pi}{6}\right), \quad (\text{A7})$$

with  $\omega = (2\sqrt{3}\mu)^{-1}$ . Therefore, by substituting these results into Eq. (A5) and integrating over time, the effective diffusion coefficient is obtained as

$$D_{\text{eff}} = D_{\text{st}} + 2(D_2 - D_1) \frac{\frac{1}{2} - B_-(t, \omega) \exp\left[-\frac{3t}{2\tau_0} e^{-\Delta U/(k_B T)}\right]}{7t \tau_0^{-1} e^{-\Delta U/(k_B T)}} + 2(D_3 - D_1) \frac{1 - B_+(t, \omega) \exp\left[-\frac{3t}{2\tau_0} e^{-\Delta U/(k_B T)}\right]}{7t \tau_0^{-1} e^{-\Delta U/(k_B T)}}. \quad (\text{A8})$$

Here, the steady-state effective diffusion coefficient is

$$D_{\text{st}} = \frac{D_1 + D_2 + D_3}{3}, \quad (\text{A9})$$

and the oscillatory terms are

$$B_{\pm}(t, \omega) = \frac{3}{2} \sin\left(\omega t \pm \frac{\pi}{6}\right) + \frac{1}{2\sqrt{3}} \cos\left(\omega t \pm \frac{\pi}{6}\right). \quad (\text{A10})$$



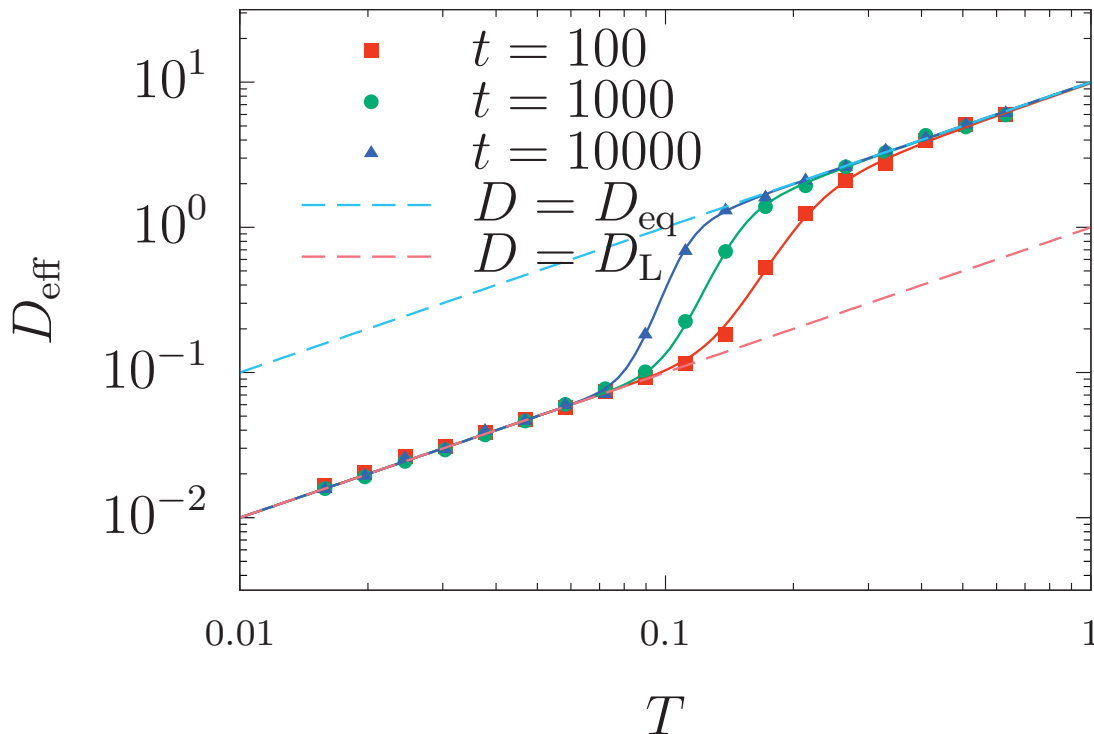


FIG. S2. Temperature-dependent effective diffusion coefficient for different observation times in the three-state model. Symbols indicate simulation results, dashed lines represent the initial and equilibrium diffusion coefficients, and solid lines show the theoretical prediction given by Eq. (A8). In the simulations, we set  $\tau_0 = 1$  and  $\Delta U = 1$ .

Equation (A8) describes how a system whose diffusion coefficient switches among three states separated by a potential barrier of height  $\Delta U$  relaxes from a nonequilibrium initial condition to the steady state. This follows directly from the behavior of  $p_2(t)$  and  $p_3(t)$  in Eqs. (A6) and (A7), which oscillate while decaying exponentially; consequently, the instantaneous diffusion coefficient relaxes as the state-occupancy probabilities approach their stationary value  $1/3$  for each state.

Figure S2 shows the temperature dependence of the effective diffusion coefficient in the three-state model. The results clearly demonstrate an observation-time-induced crossover. Even when the instantaneous diffusion coefficient has no equilibrium value, if the state distribution reaches stationarity at high temperatures or over sufficiently long observation times, the diffusion of particle positions becomes practically indistinguishable from that in equilibrium systems. Consequently, the effective diffusion coefficient exhibits a temperature crossover that depends on the observation time. In contrast, at low temperatures or over short observation times, biases from the initial condition persist and nonequilibrium behavior remains pronounced.

These results also demonstrate that the emergence of an observation-time-induced crossover requires not merely switching between two states, but the presence of two or more transition states in the instantaneous diffusion coefficient.

### III. ASYMMETRIC DOUBLE-WELL CONTROL OF DIFFUSING DIFFUSIVITY

In this section, we show that by employing an asymmetric potential for the particle radius  $r$  in the DWCD model, the theoretical framework of the two-state model can be applied to generic (asymmetric) double-well potentials. We

employ the following composite double-well potential:

$$V(r) = \begin{cases} U_L \left[ \left( \frac{r-3}{2} \right)^2 - 1 \right]^2, & \text{if } r \leq 3, \\ U_R \left[ \left( \frac{r-3}{2} \right)^2 - 1 \right]^2 + (U_L - U_R), & \text{if } r > 3, \end{cases} \quad (\text{A11})$$

where  $U_L$  and  $U_R$  control the well depths on the left and right, respectively. This potential has minima at  $r_+ = 1$  and  $r_- = 5$ , and a potential barrier at  $r_M = 3$ . By replacing the potential in Eq. (4) of the main text with the above form, we obtain an asymmetric DWCD model, enabling a more realistic description of the protein conformation via the radius of gyration  $r$ . As the initial condition for  $r$ , as in the symmetric-potential case, we set  $r(t) = r_-$  at  $t = 0$ .

When employing a composite double-well potential, one must account for the fact that the escape time depends on which well the system escapes from. According to the Arrhenius law, the mean escape times from the wells at  $r_{\pm}$  are

$$\mu_{\pm} \sim 2 \alpha_{\pm} \delta_{\pm} \pi \exp \left( \frac{V(r_M) - V(r_{\pm})}{k_B T} \right), \quad (\text{A12})$$

where  $r_M$  denotes the position of the barrier top. Here,  $\alpha_{\pm}$  are prefactors determined by the curvatures of the potential in the vicinity of  $r = r_{\pm}$ , and  $\delta_+$  ( $\delta_-$ ) is a constant computed from the curvature at  $r = r_M$  of the left (right) branch of the double-well potential. Since Eq. (14) of the main text holds generally for sojourn times with different means, by substituting the escape times given by Eq. (A12), the effective diffusion coefficient for an asymmetric potential can be computed as

$$D_{\text{eff}} = D_{\text{eq}} - (D_+ - D_-) \frac{\alpha_+ \delta_+ e^{\frac{U_L}{k_B T}}}{\alpha_+ \delta_+ e^{\frac{U_R}{k_B T}} + \alpha_- \delta_- e^{\frac{U_L}{k_B T}}} \left( \frac{1 - e^{-t/\kappa(T)}}{t/\kappa(T)} \right), \quad (\text{A13})$$

$$\kappa(T) \equiv 2 \alpha_+ \delta_+ \alpha_- \delta_- \pi e^{\frac{U_L + U_R}{k_B T}} \left( \alpha_+ \delta_+ e^{\frac{U_L}{k_B T}} + \alpha_- \delta_- e^{\frac{U_R}{k_B T}} \right)^{-1}. \quad (\text{A14})$$

Here,  $U_L$  and  $U_R$  denote the heights of the left and right potential barriers, respectively, defined as  $U_L = V(r_M) - V(r_+)$  and  $U_R = V(r_M) - V(r_-)$ .

Equation (A13) elucidates how  $D_{\text{eff}}$  relaxes toward equilibrium as a function of temperature  $T$  or observation time  $t$  when the diffusivity switches between wells of a double-well potential with unequal depths  $U_L$  and  $U_R$ . The parameter  $\kappa(T)$  sets the relaxation time of the diffusion process and, unlike the symmetric-potential case, it depends explicitly on the depths of the two wells.

*Effect of Potential Asymmetry.*—Figure S3 presents the temperature dependence of the effective diffusion coefficient  $D_{\text{eff}}$  in the DWCD model with asymmetric well depths. In all cases, theoretical predictions from Eq. (A13) (solid lines) are in excellent agreement with the simulation results (symbols). When the asymmetry is weak, an observation-time-induced crossover is clearly observed and the transition temperature depends on the observation time (panel (a)). As the asymmetry increases, this time dependence progressively weakens, and the transition temperature becomes essentially independent of the observation time (panels (b) and (c)). This can be explained as follows. As the potential asymmetry increases ( $U_L \ll U_R$ ), the equilibrium distribution of the particle radius  $r$  approaches a Gaussian peaked at  $r = r_-$ . In the strongly asymmetric limit, the equilibrium distribution can be approximated by a delta function  $\delta(r - r_-)$ , which is nearly identical to the initial distribution. Consequently, the third condition for an observation-time-induced crossover discussed in the main text—“The system is initially out of equilibrium.”—is no longer satisfied, and the transition behavior ceases to depend on the observation time. Therefore, even in asymmetric two-state systems, an observation-time-induced crossover emerges, and the three conditions presented in the main text should be regarded as necessary conditions for the occurrence of this phenomenon.

#### IV. EFFECT OF THE EQUILIBRATION TIME

In both the theoretical analysis and the simulations of the observation-time-induced crossover, we previously assumed a fully nonequilibrium initial condition, namely that the particle radius satisfies  $r = r_-$  at time  $t = 0$ . Here, we demonstrate that the observation-time-induced crossover still appears even when the system is allowed to equilibrate for a relatively long duration—comparable to the observation time—before measurements begin.

Figure S4(a) shows the simulation results for the DWCD model, where the system is allowed to equilibrate for a time exactly equal to the observation time  $t_{\text{obs}}$  before we start measuring the effective diffusion coefficient of

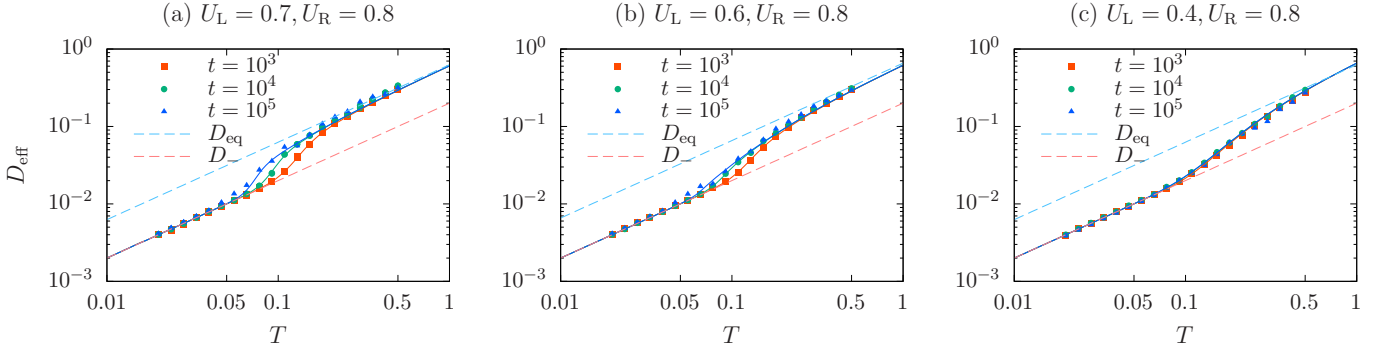


FIG. S3. Temperature-dependent effective diffusion coefficient  $D_{\text{eff}}$  for different observation times in the asymmetric DWCCD model. Each panel uses a different left-well depth  $U_L$ . Symbols indicate simulation results, dashed lines represent the initial and equilibrium diffusion coefficients, and solid lines show the theoretical prediction given by Eq. (A13).

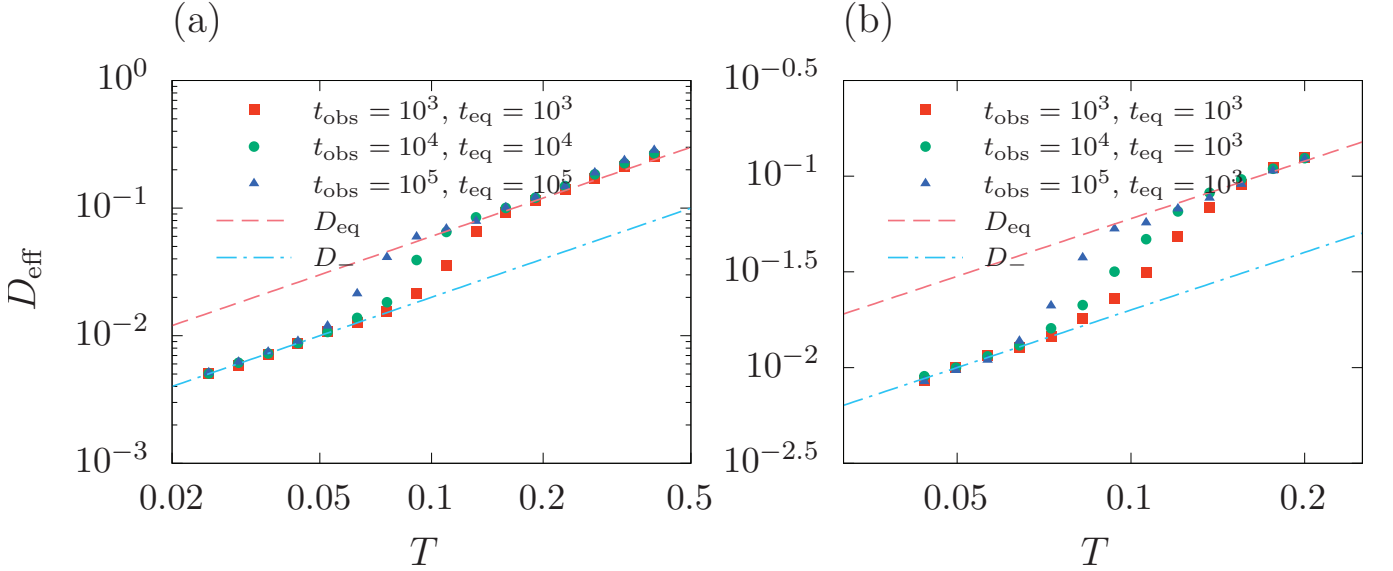


FIG. S4. (a) Temperature dependence of the effective diffusion coefficient in the DWCCD model when the system is equilibrated for a time equal to the observation time  $t_{\text{obs}}$ . (b) Temperature dependence of the effective diffusion coefficient when the equilibration time is fixed to  $t_{\text{eq}} = 10^3$ , independently of  $t_{\text{obs}}$ . In both panels, the dashed lines indicate the initial effective diffusivity  $D_-$  and the equilibrium effective diffusivity  $D_{\text{eq}}$ .

the particle. Here,  $t_{\text{eq}}$  denotes the equilibration time elapsed from the initial condition. Before this equilibration stage, the initial condition of the particle radius is fixed to  $r = r_-$ . As is evident from the results, even when such an equilibration time is introduced prior to observation, the diffusivity still exhibits a crossover as a function of temperature, and the corresponding crossover temperature depends on the observation time; that is, the observation-time-induced crossover persists. Figure S4(b) shows the results for a protocol in which the equilibration time is fixed to  $t_{\text{eq}} = 10^3$ , independently of the observation time  $t_{\text{obs}}$ . Even with this protocol, the observation-time-induced crossover is clearly observed.

## V. HEATING-COOLING ASYMMETRY IN THE DOUBLE-WELL CONTROLLED DIFFUSING DIFFUSIVITY MODEL

We next investigate the heating-cooling asymmetry in the DWCCD model by changing the initial condition of the radius  $r$ . In the simulations presented in the main text, at each temperature we imposed the initial condition  $r = r_-$  and  $x = 0$  independently for every realization. Here we instead modify the protocol so that the temperature is varied sequentially while observations are performed.

The simulation procedure is as follows. At the initial temperature  $T = T_0$ , we set the initial condition at  $t = 0$  to

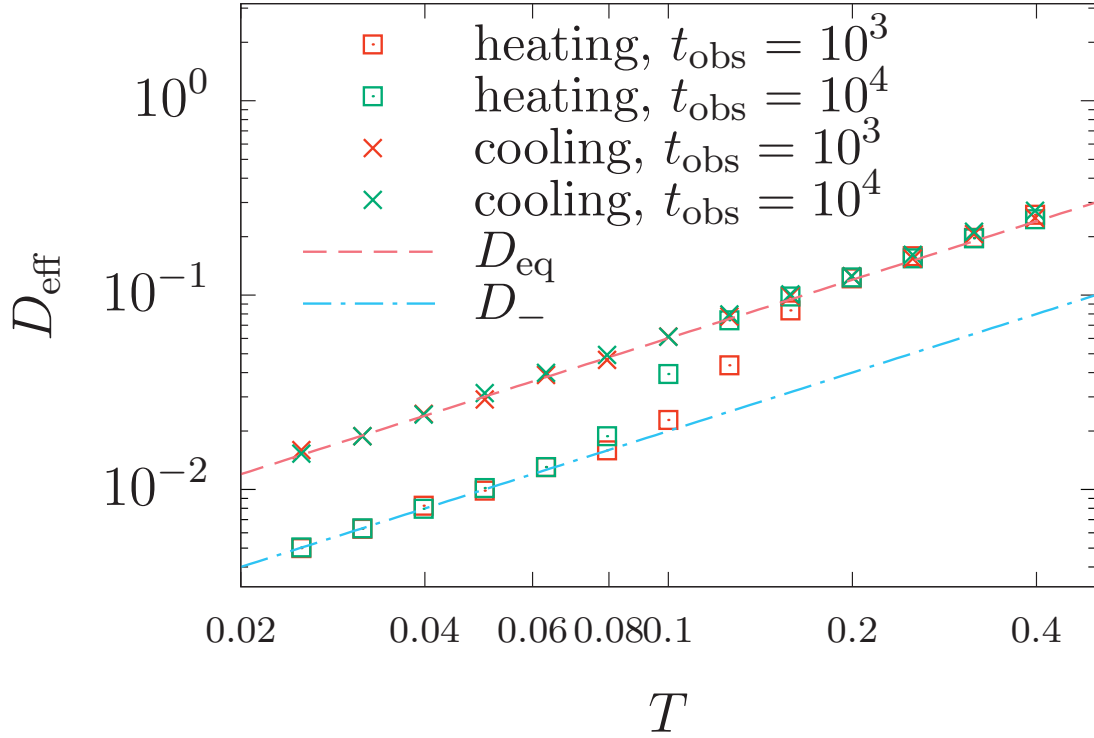


FIG. S5. Temperature dependence of the effective diffusion coefficient for the heating and cooling protocols. Squares denote the heating protocol and crosses denote the cooling protocol. The dashed lines indicate the initial effective diffusivity  $D_-$  and the equilibrium effective diffusivity  $D_{\text{eq}}$ . The initial temperature in the heating protocol is  $T_0 \simeq 0.025$ , while that in the cooling protocol is  $T_0 \simeq 0.4$ .

be  $r = r_-$  and  $x = x_0$ . After evolving the system at  $T_0$ , we change the temperature to the next value  $T = T_1$  without reinitializing  $r$  or  $x$ : the values of  $r$  and  $x$  at the end of the run at  $T_0$  are directly used as the initial condition at  $t = 0$  for the simulation at  $T_1$ . Repeating this procedure yields, for a sequentially measured set of  $N$  temperatures  $\{T_0, T_1, \dots, T_{N-1}\}$ , the effective diffusion coefficient defined from the mean-square displacement as

$$D_{\text{eff}}(t) \equiv \frac{\langle (x(t) - x(0))^2 \rangle}{2t}. \quad (\text{A15})$$

By choosing the sequence  $\{T_0, T_1, \dots, T_{N-1}\}$  in ascending or descending order, we can probe the effect of heating and cooling protocols, respectively.

Figure S5 shows the temperature dependence of the effective diffusion coefficient obtained from simulations following the protocol described above. For the heating protocol, relaxation is slow in the low-temperature regime, so the influence of the nonequilibrium initial condition persists during the measurement and the effective diffusion coefficient exhibits a crossover as a function of temperature. Moreover, when the observation time is varied, the temperature at which this crossover occurs shifts, demonstrating the observation-time-induced crossover.

By contrast, for the cooling protocol, although we impose a nonequilibrium initial condition  $r = r_-$  at the starting temperature  $T_0$ , the diffusivity relaxes rapidly in the high-temperature regime. Once the system has equilibrated at high temperature, subsequent cooling does not regenerate a significant nonequilibrium bias; instead, the system quasi-adiabatically follows the equilibrium distribution at each temperature, and the effective diffusion coefficient remains at its equilibrium value throughout the temperature range.